THE ASTROPHYSICAL JOURNAL, 400:321–329, 1992 November 20

GINGA OBSERVATIONS OF X-RAY FLARES ON ALGOL

R. A. STERN,[1,2] Y. UCHIDA,[3,4] S. TSUNETA,[4] AND F. NAGASE[5]

Received 1992 February 24; accepted 1992 May 21

ABSTRACT

The *Ginga* X-ray satellite observed Algol (β Per) for 2 days in 1989 January, including both the primary optical eclipse and most of the secondary eclipse. We derive upper limits of $\sim$20% and 10%, respectively, for the eclipsed flux fraction during the two eclipses. A large ($L_x \sim 10^{31}$ ergs s^{-1}) flare lasting over 12 hr was seen prior to and during secondary eclipse. The flare began with a peak temperature $\sim 6.7 \times 10^7$ K, gradually decaying to $\sim 3.6 \times 10^7$ K. High-temperature Fe line emission is clearly detected in the proportional counter data. The Fe line equivalent width is variable during the flare, ranging from 0.4–1.0 keV. Except for two intervals during the flare rise, the observed equivalent width is lower than predicted using solar abundances and an optically thin plasma model. Similar behavior has also been observed by *Ginga* in a large flare on UX Ari: in both events, opacity effects at line center may be playing a significant role. Loop model analysis of the large flare suggests that it involves a substantially longer loop or loops than a shorter duration Algol flare seen with *EXOSAT*. Mass ejections associated with flares of this magnitude, occurring every few days, may contribute significant amounts of material to the transient H II or higher temperature plasma regions observed in the Algol system.

Subject headings: binaries: eclipsing — stars: coronae — stars: individual (β Persei) — X-ray: stars

1. INTRODUCTION

The prototype eclipsing binary Algol (β Per), first identified as a pair of orbiting stars by Goodricke in 1782, remains an object of intense scrutiny. Algol, with a period of 2.87 days, consists of a B8 V primary (Algol A) and K2 IV secondary (Algol B) in which the secondary fills its Roche lobe. Both primary and secondary optical eclipses are partial. A recent IAU Colloquium testifies to the highly active current research on the subject of Algols in general (Batten 1989).

The Algol system was first detected in X-rays by *SAS 3* (Schnopper et al. 1976) and confirmed as an X-ray source by Harnden et al. (1977). Initial interpretations of the X-ray emission focused upon the accretion disk paradigm, since optical observations indicated that Algol B was transferring mass to Algol A. This interpretation was bolstered by the fact that most of the Galactic X-ray sources discovered up to that time were mass-transferring binary systems. However, *Einstein* Observatory SSS observations during primary optical eclipse found no evidence of an X-ray eclipse. Since the shock-heated matter passing through the inner Lagrangian point of the system would be eclipsed by the secondary, this observation suggested that Algol B accounted for most of the X-ray emission (White et al. 1980). At about this time, the RS CVn binary systems, many with evolved subgiant members similar to Algol B, were established as a class of soft X-ray emitters (Walter & Bowyer 1981). Thus the short period of the Algol system, with the rapid rotation of the secondary, could easily account for Algol's relatively low (10^{30-31} ergs s^{-1}) X-ray luminosity compared to most mass-transfer X-ray binary systems ($L_x \approx 10^{36-38}$ ergs s^{-1}).

EXOSAT observations of Algol covering the secondary optical eclipse were interpreted as evidence for a very shallow X-ray eclipse. This in turn, suggested a large scale for the X-ray emitting region (White et al. 1986). During the *EXOSAT* observation, a large flare was detected, lasting about 4 hr (White et al. 1986; van den Oord & Mewe 1989).

Algol also exhibits both steady and flaring microwave emission ranging from a few to hundreds of mJy (Gibson 1976; Hjellming & Gibson 1980). VLBI measurements indicate an extended source of dimensions $\sim$1–3 times the radius of Algol B, depending upon frequency (Lestrade et al. 1988). Algol and similar binary systems were also observed with good phase coverage using the IUE observatory. A key result of these observations was the detection of a moderately hot (10^5 K), low-density ($\sim 10^9$ cm^{-3}) region apparently surrounding the *primary* (Peters & Polidan 1984; Brandi et al. 1989). In the usual Roche lobe overflow interpretation, such regions arise from shock heating of accreting matter by the primary.

Other recent results suggest that spectroscopic and possibly other peculiarities in the Algol system are a result of intense stellar activity centered on Algol B. Hall (1989) reviews the relationship between Algol and RS CVn systems. Richards (1990), in an analysis of the Algol visible and near-IR light curve, suggested that the variability of the light curve from epoch to epoch during primary minimum could be evidence of starspots. Hα observations, too, exhibit a complicated structure as a function of orbital phase. Most of the Hα emission is attributed to various parts of an accretion disk, yet there is clearly an active and variable chromosphere on the secondary star (Richards 1992). Thus, additional observations, especially in the critical X-Ray regime, should help to shed light on the interplay between gravitational and magnetic effects in the Algol system.

Under the auspices of the NASA/ISAS *Ginga* Visiting Investigator Program, we obtained a 2-day X-ray observation of

[1] NASA/ISAS *Ginga* Visiting Investigator.
[2] Solar and Astrophysics Laboratory, 0/91-30, Building 252, Lockheed Palo Alto Research Laboratory, 3251 Hanover Street, Palo Alto, CA 94304.
[3] Department of Astronomy, University of Tokyo, 3-1 Hongo 7-chome, Bunkyo-ku, Tokyo 113, Japan.
[4] Institute of Astronomy, University of Tokyo, 3-1 Hongo 7-chome, Bunkyo-ku, Tokyo 113, Japan.
[5] Institute of Space and Astronautical Science, 3-1-1 Yoshino-dai, Sagamihara, Kanagawa 229, Japan.

Algol in January of 1989, including coverage of the entire primary eclipse and most of the secondary eclipse. In § 2 we describe the *Ginga* observations, in § 3 we analyze and discuss the X-ray light curve, which includes two X-ray flares, one much larger than the other, in § 4 we analyze the flare X-ray pulse height spectra, in § 5 we discuss the large X-ray flare in the context of magnetic loop scaling laws, in § 6 we discuss our observations and analysis in the context of observations in other wavebands, and in § 7 we summarize our results.

2. X-RAY OBSERVATIONS

The *Ginga* observation of Algol began at 2128 UT on 1989 January 12 and ended at 1803 UT on 1989 January 14. A nearby background region ($\sim 3\overset{\circ}{.}0$ away) was observed from 0226 to 1039 UT on 1989 January 15. All X-ray data were obtained with the LAC (Large Area Counter) instrument. The LAC consists of eight sealed Be-window collimated proportional counters having a total peak effective area of ~ 4000 cm^2 and a $1\overset{\circ}{.}08 \times 2\overset{\circ}{.}0$ FWHM field of view. The LAC responds to X-rays in the range 1.2–37 keV with an energy resolution of 18% FWHM at 5.9 keV. A detailed description of the LAC is given by Turner et al. (1989). A description of the *Ginga* satellite is given in Makino & ASTRO-C Team (1987).

The *Ginga* LAC observation of Algol is somewhat complicated by the nearby presence of the Perseus Cluster. The LAC field-of-view (FOV) roll angle in the sky is constrained by the fixed orientations of the solar panels, the source line of sight (LOS), and the Sun position on a given date. For our Algol observation, Perseus lies $\approx 2\overset{\circ}{.}2$ away from the instrument LOS along the long FOV axis, and $0\overset{\circ}{.}9$ away from the LOS along the short FOV axis. Referring to Turner et al. (1989), this would result in an off-axis response well below 10%, probably only a few percent for a point source; however, since the Perseus cluster is both extended ($\gtrsim 1°$) and a strong source (≈ 50 mCrab) with a harder spectrum than Algol, a significant contribution to the quiescent Algol flux is likely. This may have been observed in the quiescent pulse-height spectrum (see § 4). The Perseus cluster contribution is not a problem for flare spectra, as the pre-flare quiescent Algol flux is subtracted prior to model fitting.

At 1010 UT on January 13, a solar flare was detected by the *Ginga* Gamma-Ray Burst Detector (Murakami et al. 1989; T. Murakami 1989, private communication). LAC data for ≈ 15 minutes immediately prior to and including the burst were removed from the Algol observation data. Correlations of LAC count rate with the bright earth limb and regions of very high particle fluxes (low magnetic rigidity regions) were used to determine data exclusion regions.

The light curve and spectral data were extracted using the procedure of Hayashida et al. (1989); details of how this method is employed can be found in that reference and in Stern et al. (1992) for σ^2 CrB, a much weaker source. Because the *Ginga* orbit has slowly decayed since launch in 1987 February due to an unexpectedly strong period of solar activity, a modified background subtraction procedure was developed by K. Hayashida (1989, private communication), involving a correction for six of the eight LAC detector modules. Comparison of the light curves obtained from this latter procedure and the original technique show minimal differences in the case of the Algol observation. Therefore the full eight-counter summed light curve is used in the following analysis.

3. X-RAY LIGHT CURVE

3.1. *Overall X-Ray Light Curve*

The background-subtracted X-ray light curve (1.2–18 keV) for the Algol observation is shown in Figure 1. The approximate times of primary and secondary eclipse and the respective 1st and 4th contact points are also shown in the figure. We used the same ephemeris as given by White et al. (1986): this should be accurate to a time scale of a few minutes.

The features of the light curve are as follows: (1) a relatively quiescent period during primary eclipse on January 13, with a slowly declining flux; (2) a small flare at about 1300–1600 UT on January 13 following primary eclipse; and, most notably, (3) a large X-ray flare of unusually long duration, over half a day, beginning at about 0200 UT on January 14 and continuing through secondary eclipse to the end of the *Ginga* observation.

3.2. *Limits on Eclipses*

In Figure 2*a* we show an expanded light curve for the period of primary eclipse. We fitted the X-ray light curve over this period with a simple linear function of time. The residuals are plotted in Figure 2*b*, with the eclipse times shown. We note that, although there is a suggestive dip near mid-eclipse in the residuals plot, the variability of the source may be influencing our results. We conservatively estimate any possible eclipsed fraction at about 20% of the flux. However, we must also consider the possible contribution of the Perseus cluster to the uneclipsed flux. Since any correction to the Algol flux due to Perseus is very uncertain, one way to at least estimate this effect is to examine the lowest LAC energy channels, where the contribution from the higher temperature Perseus component (see next section) is the smallest. For the 1.2–5.8 keV band, the Algol count rate is $\approx 80\%$ of the 1.2–18 keV rate, but any possible decrease in count rate at mid-primary eclipse is $\lesssim 2$ counts s^{-1}, still well within our estimated upper limits of a 20% flux decrease. This suggests that our derivation of the eclipse upper limits is not being seriously affected by the off-axis Perseus flux.

In Figures 3*a*–3*b* we show a similar set of plots for the secondary eclipse, which begins well into the large flare. In this case, we have found that an exponentially decaying light curve roughly fits the data, with an *e*-folding time scale $= 2.2 \times 10^4$ s.

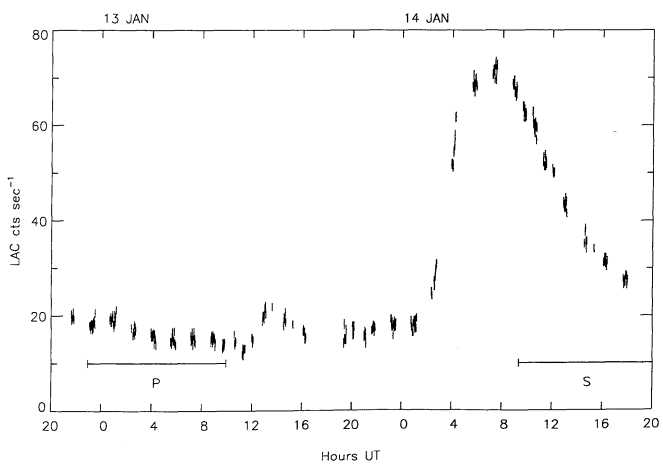

FIG. 1.—X-ray light curve (1.2–18 keV, 128 s bins, $\pm 1\ \sigma$ errors) for Algol observation. Midpoints of primary (P) and secondary (S) optical eclipses are indicated. Solid bars indicate approximate eclipse duration.

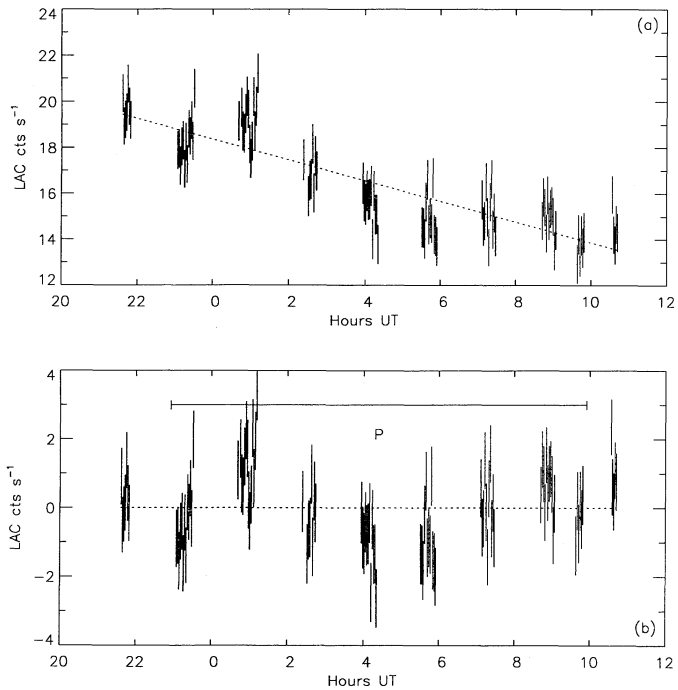

FIG. 2.—(*a*) Expanded X-ray light curve during primary eclipse. Linear fit to data is shown as dashed line. (*b*) Fit residuals. Solid horizontal bar indicates duration of primary eclipse (1st to 4th contact): "P" indicates approximate point of mid-eclipse.

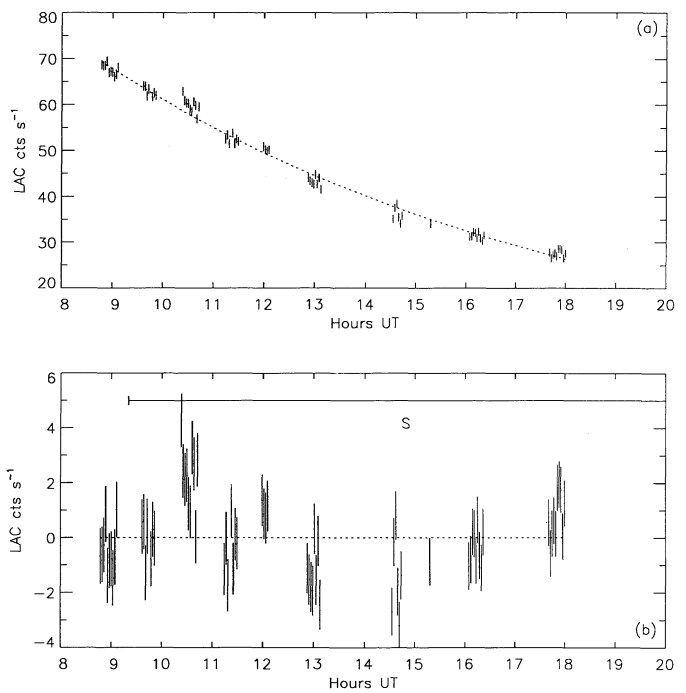

FIG. 3.—(*a*) Expanded X-ray light curve during secondary eclipse. Exponential fit to data is shown by dashed line; (*b*) fit residuals. Solid horizontal bar indicates duration of secondary eclipse: "S" indicates approximate time of mid-eclipse.

The formal fit confidence is less than 10%: much of this may well be due to shorter time scale variability, as can be seen in the plot of the fit residuals. There is some marginal evidence for a decrease in the X-ray flux during the secondary eclipse. In this instance, we again place a conservative upper limit of $\approx 10\%$ of the flux. Given the fact that the average flux during secondary eclipse is approximately 3.5 times the quiescent flux, this limit applies primarily to eclipsing of the flaring region.

4. ANALYSIS OF X-RAY PULSE HEIGHT SPECTRA

4.1. *Quiescent Spectrum*

The light curve of Algol is relatively quiescent from ≈ 2100 UT on January 12 through ≈ 1130 UT on January 13. For the purposes of spectral analysis, we have divided the data during this time period into five consecutive groups, labeled as Q1–Q5 in Figure 4.

In Table 1 we show the approximate time intervals of the Q1–Q5 samples, the effective integration time, average LAC counts s^{-1}, and χ^2_ν-values for various model fits. We attempted to fit each spectrum with: (1) single-temperature thermal bremsstrahlung models (1T), (2) 1T + Gaussian Fe line at 6.7 keV (1T + G), (3) two-temperature thermal bremsstrahlung (2T), and (4) 2T + Gaussian Fe line (2T + G). Of these models, only those with two-temperature components provided an adequate fit, with little difference between the 2T and the 2T + G models.

In Table 2 we show the best-fit model parameters for the 2T models. As indicated above, since the 2T and 2T + G models appear to fit equally well, there is no firm evidence for the presence of Fe-line emission in the quiescent data. Note that the temperature required for the lower (by a factor of 4 or more) emission measure component in the 2T fits is ≈ 50–150 MK, with large uncertainties. Because of the presence of the Perseus Cluster at the edge of the LAC field of view, and the derived spectral parameters for the Perseus Cluster from *Ginga* observations ($T \approx 73 \times 10^6$ K; Allen et al. 1992; Y. Kamata 1992, private communication), it is likely that such a high temperature component in the quiescent state is entirely due to the Perseus Cluster. This prevents us from determining the presence or absence of an $\sim 10^8$ K component in Algol similar to that detected by Doyle, van den Oord, & Kellett (1992) in a *Ginga* observation of II Peg.

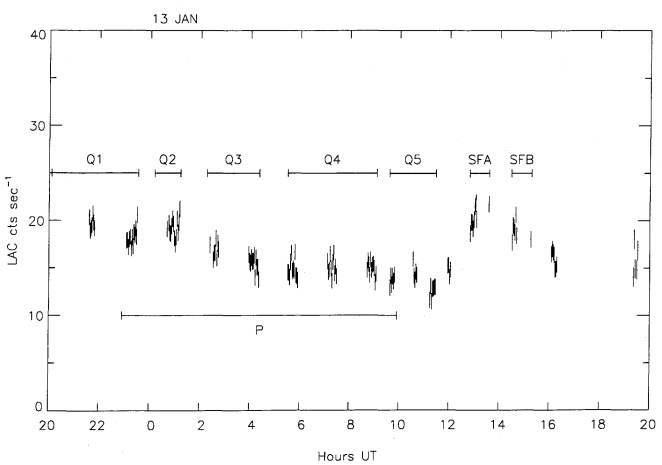

FIG. 4.—Time intervals selected for quiescent (Q1–Q5) and small flare (SFA–SFB) spectral extractions. Primary eclipse is indicated as in Fig. 2.

TABLE 1

QUIESCENT SPECTRAL FITS[a]

SPECTRUM LABEL	DAY	START (UT)	STOP (UT)	EFFECTIVE TIME (s)	χ^2_ν 1T $\nu = 28$	2T $\nu = 26$	1T + G $\nu = 27$	2T + G $\nu = 25$
Q1	12 Jan	20:06	23:32	3226	5.9	1.2	5.2	1.2
Q2	13 Jan	00:11	1:13	2013	4.6	1.7	4.0	1.7
Q3	13 Jan	2:16	4:22	3043	6.1	1.1	5.7	1.2
Q4	13 Jan	5:30	9:06	4018	9.2	1.4	6.9	1.0
Q5	13 Jan	9:37	11:28	2075	2.7	0.8	2.1	0.7

[a] PHA channels 2–31 used.

The higher temperature fit component appears to increase in temperature (with admittedly large uncertainties) and decrease in emission measure during the periods Q3 and Q4 (the primary optical eclipse), while the lower temperature component remains relatively unchanged. Unfortunately, the Perseus cluster spectral contamination prevents us from drawing any unambiguous conclusions from this result. In any case, since the *Ginga* observation of primary eclipse is the first since the original *Einstein* observations of White et al. (1980), it may be worthwhile to study the primary eclipse with the next generation of X-ray satellites with imaging detectors, to see if a hard component does exist.

The presence of the Perseus cluster component in our spectra may also be influencing the estimated 15 MK temperature for the lower temperature component. However, it is worth noting that temperature estimates for Algol vary widely among previous investigations using different instruments or different models with the same instrument. For example, White et al. (1980) and Swank et al. (1981), using *Einstein* SSS data (0.5–4 keV), report temperatures of roughly 8 and 40 MK for a 2T Raymond-Smith model. White et al. (1986), using the *EXOSAT* ME (1–10 keV), found that a 1T thermal bremsstrahlung model of ~25 MK adequately fit their data. A later analysis of the same ME data by Pasquini, Schmitt, & Pallavicini (1989) using a 2T Mewe model, found temperatures of 7 and 39 MK, very similar to the *Einstein* SSS results. We also note that our 1T models, although they represent poor fits to the *Ginga* quiescent data, produce temperature estimates of ~27–35 MK, in closer agreement with the *EXOSAT* ME data and the SSS higher temperature component. Given the limited bandpass of each detector, it is likely that these variations in model parameters are at least as much due to the detector and model variations as to any real change in Algol's spectrum.

4.2. *Small Flare*

Beginning sometime after ≈1200 UT on January 13, the Algol count rate increases by ≈50% on the time scale of about 1 hr, returning to the "quiescent" level over a period of 4–6 hr. This enhancement has all the markings of a small flare. To see if the plasma temperature increases during this purported flare event, we fit the LAC pulse height spectrum to 2 time intervals, after having subtracted a pre-flare quiescent spectrum. The intervals selected are shown in Figure 4. Details of the extracted samples and model fit results are given in Table 3. To determine possible upper limits to any Fe-line flux, we fit these spectra to a combination of thermal bremsstrahlung + gaunt factor with a fixed energy (6.7 keV) Fe-line. Good fits were obtained at flare peak (SFA) and the beginning of the decay (SFB), indicating a decrease in temperature from 77 ± 21 to 43 ± 13 MK. The emission measure is about one order of magnitude lower than the large flare seen later in the *Ginga* observation. The 90% confidence upper limits for the Fe-line equivalent width for this flare are marginally consistent with that expected from theory (see § 6).

TABLE 2

BEST-FIT PARAMETERS: QUIESCENT DATA[a]

Label	T_1 (10^6 K)	EM_1 (10^{53} cm^{-3})	T_2 (10^6 K)	EM_2 (10^{53} cm^{-3})
Q1	15. ± 2.	7.7 ± 1.3	75 ± 16	1.5 ± 0.5
Q2	15. ± 3.	6.9 ± 1.2	74 ± 21	1.8 ± 0.6
Q3	17. ± 2.	6.9 ± 0.7	150 ± 100	0.3 ± 0.3
Q4	15. ± 2.	7.9 ± 0.9	130 ± 60	0.8 ± 0.2
Q5	12. ± 2.	6.9 ± 1.5	57 ± 22	1.4 ± 0.6

[a] 90% confidence limits, one parameter.

4.3. *Large Flare*

For the large flare, we summed the X-ray pulse-height spectra into 11 time intervals roughly corresponding to the groups of contiguous data seen in the X-ray light curve. These are indicated in Figure 5. Before model-fitting, we subtracted the quiescent spectrum corresponding to ~1800–2300 UT on January 13. All the resultant spectra were adequately modeled by a thermal bremsstrahlung spectrum + Fe line emission. A list of the extracted times, χ^2 values, best-fit model parameters and derived quantities such as emission measure and equivalent width are given in Table 4. Examples of fitted spectra are

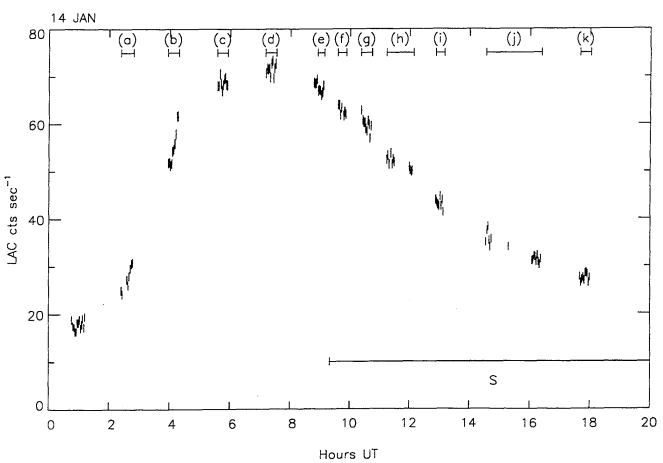

FIG. 5.—Time intervals selected for large flare spectral extractions (*a–k*). Secondary eclipse is indicated as in Fig. 3.

TABLE 3

SMALL FLARE FITS

Spectrum Label	Start (Jan 13 UT)	Stop (Jan 13 UT)	Effective Time (s)	χ^2_ν	T (10^6 K)	EM (10^{53} cm^{-3})	Fe EW[a] (keV)
SFA.....	12:49	13:36	1028	1.0	77. ± 21.	1.3 ± 0.2	≤0.6
SFB.....	14:29	15:17	799	1.2	43. ± 13.	1.5 ± 0.3	≤1.3

[a] Line energy fixed at 6.7 keV.

shown in Figure 6. In Figure 7 we show the derived temperature, emission measure (EM = $n_e^2 V$), the Fe line equivalent width, and the ratio of EM/$T^{13/4}$ (see § 5) as a function of time for the large flare.

5. ANALYSIS OF LARGE FLARE

Using the measured temperatures, emission measures, and decay time scales, we may derive estimates for the flare parameters, once we have assumed a particular form of the flare cooling. Such estimates have been based upon scenarios of, e.g., equal time scales for conductive and radiative cooling (Moore et al. 1980; Stern, Underwood, & Antiochos 1983), or a functional form in which one must guess at the dominant cooling mechanism based upon estimates of loop size (e.g., van den Oord, Mewe, & Brinkman 1988). For the Algol flare detected by *EXOSAT*, radiative cooling appeared to dominate, given the flare's size and duration (White et al. 1986; van den Oord & Mewe 1989): this is likely the case for the present Algol flare, given its even larger size and longer duration.

The relevant e-folding time scales for the flare decay are as follows: temperature, $\tau_T \approx 52{,}800$ s, luminosity, $\tau_{L_x} \approx 20{,}000$ s, and emission measure, $\tau_{EM} \approx 22{,}100$ s. For comparison purposes, this results in an effective e-folding time scale (as defined by van den Oord et al. 1988) of ≈25,500 s. The rise times for L_x and EM are about a factor of 3 shorter than the corresponding decay times, depending upon what functional form is used to parameterize the rising portion of the light curve. Under the radiative cooling hypothesis, the derived flare parameters are as follows: electron density $n_e \approx 6.5 \times 10^{10}$ cm^{-3}; loop length $L \approx 4.3 \times 10^{11}[N\alpha_{0.1}^{-2}(\Gamma + 1)]^{(-1/3)}$ cm, where N = number of loops, α = loop aspect ratio (normalized to 0.1), Γ = loop expansion factor (see e.g., van den Oord et al. 1988 for equations used to derive these quantities).

With the excellent *Ginga* time history of the Algol flare parameters, there are, in addition, significantly more constraints which we may place upon the flare parameters and geometry given the slowly evolving nature of the flare near the peak of the emission measure curve and during the flare decay. In many previous papers on stellar flare analysis (e.g., Stern, Antiochos, & Underwood 1983; Haisch 1983; White et al. 1986), magnetic loops were implicitly assumed in deriving flare parameters. However, because of the dynamic nature of flares,

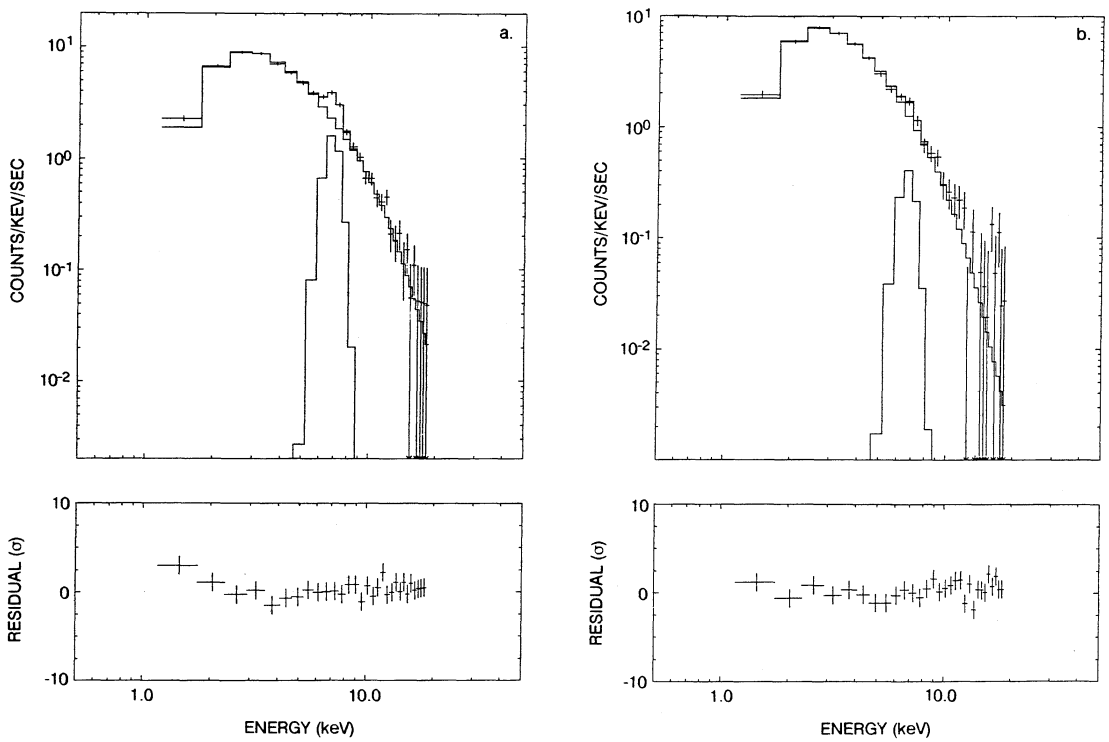

FIG. 6.—(*upper graphs*) Representative pulse-height spectra during large flare. (*a*) Rise phase: 0356–0418 UT, (*b*) decay phase: 1252–1309 UT. Data are indicated by crosses with error bars. Model fit includes two components: thermal bremsstrahlung and Fe line. Solid lines indicate each component and net model spectrum. (*lower graphs*) Spectrum fit residuals (σ).

TABLE 4

LARGE ALGOL FLARE FITS[a]

Spectrum Label	Start (UT)	Stop (UT)	T (10^6 K)	χ^2_ν	L_x (10^{30} ergs s^{-1})	EM 10^{53} cm^{-3})	E_{line} (keV)	Equivalent Width (keV)
(a)	2:23	2:48	66.7 ± 11.6	1.1	2.1 ± 0.2	2.3 ± 0.2	6.56 ± 0.25	0.93 ± 0.25
(b)	3:56	4:18	60.1 ± 2.8	1.1	7.2 ± 0.2	8.3 ± 0.2	6.63 ± 0.07	1.00 ± 0.08
(c)	5:34	5:55	61.8 ± 2.2	1.3	9.7 ± 0.2	11.4 ± 0.3	6.75 ± 0.10	0.52 ± 0.04
(d)	7:10	7:32	54.8 ± 1.7	1.1	10.1 ± 0.2	13.0 ± 0.2	6.68 ± 0.09	0.59 ± 0.05
(e)	8:55	9:08	46.8 ± 1.9	1.0	9.2 ± 0.3	13.4 ± 0.3	6.66 ± 0.12	0.60 ± 0.08
(f)	9:35	9:52	45.5 ± 1.9	1.4	8.3 ± 0.3	12.8 ± 0.4	6.71 ± 0.14	0.56 ± 0.08
(g)	10:22	10:44	43.2 ± 1.5	1.6	7.7 ± 0.2	12.5 ± 0.4	6.65 ± 0.18	0.42 ± 0.08
(h)	11:13	12:07	41.1 ± 1.7	1.6	6.2 ± 0.2	10.6 ± 0.4	6.71 ± 0.20	0.43 ± 0.09
(i)	12:52	13:09	37.6 ± 2.1	1.3	4.7 ± 0.2	8.7 ± 0.4	6.47 ± 0.29	0.43 ± 0.10
(j)	14:32	16:23	35.3 ± 2.9	1.2	2.9 ± 0.2	5.9 ± 0.3	6.73 ± 0.34	0.53 ± 0.20
(k)	17:40	18:01	35.6 ± 4.1	1.4	1.9 ± 0.2	3.8 ± 0.4	7.28 ± 0.60	0.48 ± 0.40

[a] 90% confidence limits, one parameter.

the "static" scaling laws for nonflare magnetic loops developed by Landini & Monsignori-Fossi (1975), Rosner, Tucker, & Vaiana (1978), Craig, McClymont & Underwood (1978), and Vesecky, Antiochos, & Underwood (1979) were not directly applied.

Some researchers have also investigated detailed hydrodynamic modeling of flare loops in the Sun and stars (e.g., Pallavicini et al. 1983; Peres et al. 1987; Reale et al. 1988). For compact flares, a slightly different approach was taken by Kopp & Poletto (1990). The use of detailed hydrodynamic codes as applied to stellar flares is somewhat controversial, since many of the preflare parameters are not available from integrated disk stellar X-ray observations. Even in the solar case, many assumptions must be made concerning the time history and magnitude of the flare heating event: usually the flare is assumed to begin with a heating spike or rapid rise (reasonable), with an abrupt cutoff to the flare heating near the flare emission measure peak (questionable?).

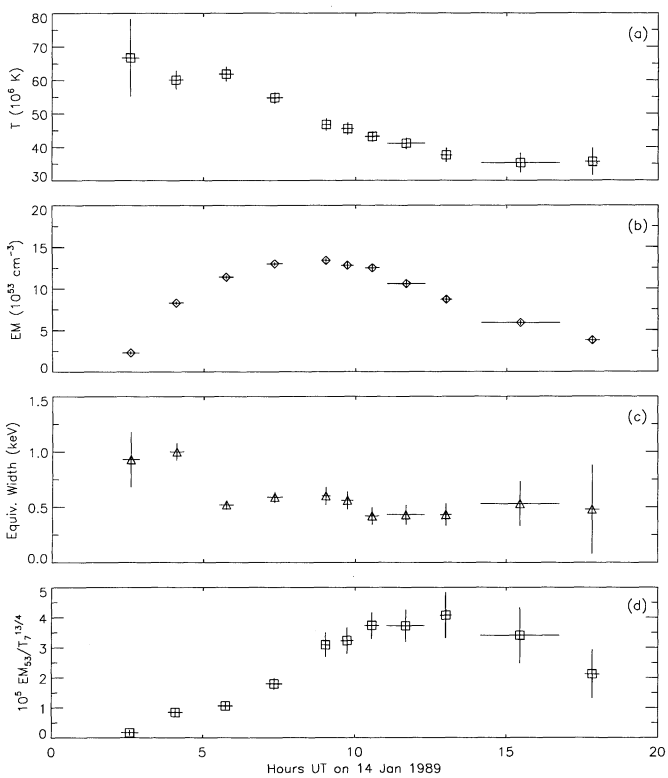

FIG. 7.—Large flare: (*a*) temperature (MK), (*b*) emission measure (10^{53} cm^{-3}), (*c*) Fe-line equivalent width (keV), and (*d*) normalized ratio of τ_c/τ_r (see text). All errors are 90% confidence, single parameter.

However, in two recent papers by van den Oord & Mewe (1989) and Fisher & Hawley (1990), a modified approach is pursued, which allows additional constraints to be placed on the flare parameters without adding in too many additional assumptions. In effect, the same loop scaling laws used to relate the pressure, length, and temperature of static loops are applied to the initial decay phase of a flare. At first glance, the use of an essentially equilibrium model during a nonequilibrium event such as a flare would seem to be a prescription for trouble. But, as the above authors have pointed out (in slightly differing fashions), near the peak of thermal X-ray emission of a flare and continuing into the early decay phase, the flare plasma approaches a so-called "quasi-static" condition, in which the ratio of radiative to conductive time scales in the loop is changing only very slowly, if at all. This condition is the same as assumed in the derivation of static loops scaling laws. Hence the flare decay can be modeled using an "equivalent" static loop.[6] The importance of this approach is that it allows an additional constraint to be placed upon the flare plasma parameters. In doing so, it is possible to derive geometrical information about the flare loops, in particular the length scale. Without the use of such scaling laws, and the time scale for flare evolution, this parameter cannot be independently determined.

As van den Oord & Mewe (1989) have pointed out, the ratio of radiative to conductive time scales for a static loop (assumed, for the moment, to be of uniform cross section) is a function only of the exponent of the temperature dependence of the radiative losses $\Lambda = n_e^2 \Psi_0 T^{-\gamma}$ (e.g., Landini & Monsignori-Fossi 1990). For $T > 20$ MK, γ has a constant value of ≈ -0.25, and $\mu = \tau_r/\tau_c \approx 0.18$. Given the observed loop parameters of T and EM, the empirical constancy of this ratio can also be checked for a given flare (to within an overall scaling factor) by taking the ratio (van den Oord & Mewe 1989)

$$\mu' \propto \frac{T_7^{13/4}}{\mathrm{EM}_{53}} = \text{constant}$$

[6] Fisher & Hawley (1990) go on to model *all* phases of a flare with the same formalism, demonstrating that the flare evolution equation need only be modified by a single parameter Ω of order 1 which varies depending upon the phase of the flare.

where, for convenience, we use T in units of 10^7 K and EM in units of 10^{53} cm^{-3}. In Figure 7*d* we show the inverse of this ratio during the course of the Algol flare. For comparison, we also show in Figure 7*b* the time evolution of the flare emission measure. It can easily be seen that near the peak of the flare and during the early part of the decay phase, the "quasi-static" cooling approximation is valid, and loop scaling laws may be used.

A simple comparison between the parameters derived by van den Oord & Mewe (1989) for the *EXOSAT* Algol flare, and those derived for the present *Ginga* flare on Algol demonstrates that the major difference in the two flares must be in the length scale of the loops involved. To see this, we note that the flare parameters near the start of the decay phase (peak EM) for the *EXOSAT* and *Ginga* flares are very similar (65 ± 10 vs. 55 ± 2 MK, 10 vs. 13×10^{53}), but the effective decay time of the *Ginga* flare is about 4 times longer (5600 vs. 22,500 s). In the loop scaling law models, the ratio of radiative to conductive cooling times is constant for $T > 20$ MK, giving rise to a scaling law of the form (e.g., van den Oord & Mewe 1989)

$$n_A L \propto T_A^{(2\gamma+7)/4} ,$$

where the subscript A refers to the loop apex, where the bulk of the emitting plasma is located. Since the radiative cooling time is given by

$$\tau_r \propto \frac{T^{(1+\gamma)}}{n} ,$$

it is immediately clear that $L \propto \tau T^{7/8}$ (for $\gamma = -0.25$). Thus the length scale of the loop(s) involved in the *Ginga* flare must be ≈ 4 times that of the loop length(s) in the *EXOSAT* flare. The density must be ≈ 5 times lower (to satisfy the loop scaling laws at the two temperatures). This results in a loop length of $\approx 6 \times 10^{11}$ cm and a density of $\approx 5 \times 10^{10}$ cm^{-3}, in good agreement with the density obtained earlier (6.5×10^{10} cm^{-3}) by assuming that the loop was cooling primarily through radiation. The loop height is then 2×10^{11} cm $= 2.9\, R_\odot \approx 0.8\, R_*$.

Once the density and length of the loop is determined, deriving the remaining geometrical parameter, $\rho = N_{\rm loops}\, \alpha^2(\Gamma + 1)$, is straightforward from the definition of emission measure:

$$\mathrm{EM} \approx \frac{\pi}{8} n_e^2 L^3 (\Gamma + 1) N_{\rm loops}\, \alpha^2 .$$

This yields $\rho \approx 6 \times 10^{-3}$ (since the scaling laws are a weak function of Γ, this value is only approximate). For even small values of Γ, this suggests that at most a few large loops were involved.

6. DISCUSSION

6.1. *Large Flare Characteristics*

The flare peak temperature is about a factor of 3 hotter than that of the largest solar flares, though comparable with $T_{\rm max}$ in the *EXOSAT* flare. In the *Ginga* flare, the peak temperature is reached at or near the beginning of the flare, nearly 6 hr before the EM peak. From the results of the preceding section, this is likely the result of the large loop size scale for the flare, producing a gradual density buildup from chromospheric evaporation. The closest solar analogy may be an extreme version of a two-ribbon flare. However, in attempting to identify this extremely long-duration flare on an eclipsing binary system such as Algol with a solar event, we may be pushing the "solar" analogy a bit too far. It is also worthwhile to remember that the surface gravity on the Algol K2 IV secondary is 15 times lower than on the Sun. Hence, while the physical processes which initiate and influence the flare's development may well be the same as in the case of the Sun, the flare geometry may be so different that discussion of a "two-ribbon" flare may not have much substance in fact. We certainly know, however, that the Algol flare is not likely to be "compact" in any sense!

6.2. Fe-*Line Emission*

In Figure 8 we show the measured Fe line equivalent width (EW) for both flares plotted against temperature and compared with the theoretical calculations of Rothenflug & Arnaud (1985) for a solar-abundance thin plasma. The observed and predicted values are in substantial disagreement for the lower temperature data taken during the large flare decay phase. This is in contrast to the much shorter duration *EXOSAT* flare seen by White et al. (1986), where the measured EW was consistent with theory, albeit with much greater uncertainty than in the large *Ginga* flare. The small *Ginga* flare upper limits are marginally consistent with the theoretical curve. Tsuru et al. (1989) have seen a similarly variable Fe-line equivalent width in *Ginga* observations of two large, long duration ($\tau \sim 20{,}000$ and 70,000 s) flares on UX Ari. Doyle et al. (1991) measured an Fe-line abundance only $\approx 33\%$ of solar during a much shorter duration (~ 2000 s) flare on II Peg. However, the Fe-line abundance did not vary significantly during the flare, which was only observed during the decay phase.

For the large Algol flare observed with *Ginga*, nonequilibrium effects are probably ruled out because of the long time scale and the lack of noticeable shift in the Fe-line centroid to lower ionization stages during the rise phase of the flare. Continuous absorption is not likely, as the low-energy portion of

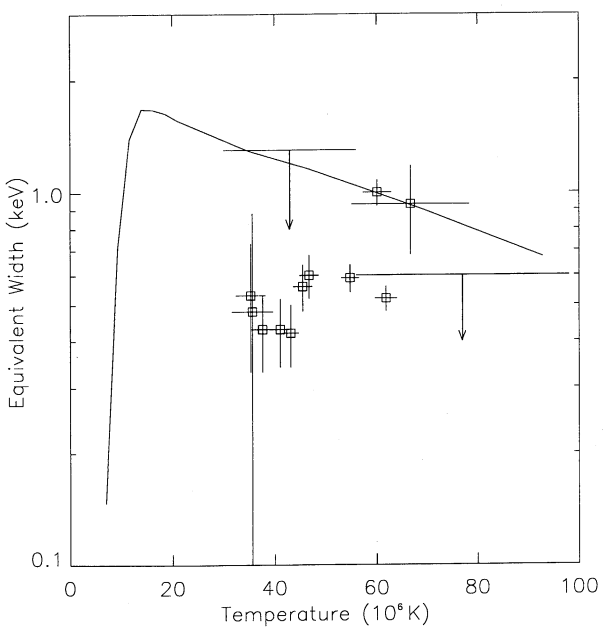

FIG. 8.—Equivalent width of Fe line plotted against continuum temperature for large flare (*boxes with 90% error bars*), and 90% upper limits from small flare (*arrows*). Solid line indicates theoretical calculations for solar-abundance thin plasma (Rothenflug & Arnaud 1985).

the X-ray spectrum does not show evidence of any cutoff. For the UX Ari flares, Tsuru et al. (1989) suggested resonance scattering as a possible explanation for the Fe-line anomaly. This scenario would require an asymmetric structure (i.e., a loop?) which is opaque at line center along the line of sight, remaining optically thin in the continuum. Using the results of Acton (1978), and Rothenflug & Arnaud (1985), we estimate $\tau_0 \approx 1$ at line center for Fe XXV at a column density $n_e l \approx 3 \times 10^{21}$ cm^{-2}. For the large Algol flare, the derived n_e of $\approx 2 \times 10^{10}$ cm^{-3} requires a column length of $\sim 1.5 \times 10^{11}$ cm to achieve $\tau_0 = 1$. This is comparable to the loop height derived above. Thus line opacity effects could be important under these conditions. However, the resonance line contribution to the Fe XXV/XXVI emission is at most $\frac{2}{3}$ of the total (Rothenflug & Arnaud 1985), so reductions of a factor of 5, as seen in the UX Ari flare, cannot be entirely explained by this mechanism (Tsuru et al. 1989). The Fe line variability may also be related to that seen in Ca XIX during solar flares, which have been attributed to abundance changes resulting from the flare heating process (Sylwester, Lemen, & Mewe 1984).

6.3. *Relationship to Observations in Other Wavelength Bands*

Algol has, of course, been extensively observed in other regions of the electromagnetic spectrum, from the microwave through the space ultraviolet. How are these observations related to the quiescent X-ray emission and, in particular, the large X-ray flares seen in the system? Obvious relationships between observed long-duration microwave flares (Gibson 1976) should exist; however, the only near-simultaneous radio-X-ray observation of Algol failed to detect an associated microwave flux increase at the beginning of the *EXOSAT* X-ray flare (van den Oord & Mewe 1989).

Richards (1990) performed an extensive analysis of the 1.2 μm infrared light curve of Algol. She finds evidence of a photometric distortion of the light curve which appears as changes in both the depths and phases of the eclipses, and an asymmetric shape to the secondary eclipse minimum. Richards attributes these distortions to starspots on the K2 IV secondary. In an RS CVn system where both stars are relatively "cool," similar starspots are generally thought to be the source of the "photometric wave" (e.g., Eaton & Hall 1979). Given the high level of (coronal) X-ray activity in Algol, it is hardly surprising, yet certainly reassuring, that RS CVn-like phenomena are observed. Hall (1989) has reviewed these similarities between Algols in general and RS CVn binaries, postulating in addition that the alternating period changes observed in some Algols are associated with the stellar magnetic cycle.

Does similar evidence for stellar activity exist in the ultraviolet region? Here the picture is significantly complicated by the presence of the B8 V primary, which dominates the UV spectrum. Hence, unlike the RS CVn systems, whose UV signatures are invariably seen in emission, *IUE* observations of Algol show evidence of *absorption* lines from 10^5 K gas (Cugier & Molaro 1984; Brandi et al. 1989). More importantly, such gas is seen with velocities characteristic of the *primary* star, hence it cannot be connected with a transition region at the base of the K star's X-ray corona.

Considerable evidence also exists for the presence of a transient H II accretion disk related to the high-temperature region and also surrounding the primary (Richards 1990). This disk is composed of a high-density ($N_e \approx 10^{11}$ cm^{-3}) Hα region, and a high rotational velocity region ($v \approx 200$–500 km s^{-1}), in addition to the high-temperature region seen in the UV. Richards attributes all of the disk's regions to the impact of the Roche-lobe transfer stream on the primary star, creating shocked gas at significant distances from the primary surface. She estimates the following parameters for the H II disk: $T \sim 10^4$ K, $N_e \sim 10^{10}$ cm^{-3}, and mass $\sim 10^{-12}\ M_\odot$.

Although both the theoretical and observational evidence for Roche-lobe overflow as the major source of the disk mass is fairly well-established, it is worthwhile, in light of the intense X-ray activity on the K subgiant, to consider an alternative source of matter which may feed the disk, at least in part. This is the Algol equivalent of solar coronal mass ejections, or CMEs. CMEs are seen on the Sun as looplike features of about 1 $R_\odot$ in white-light coronograph images, occurring at the rate of almost one per day, and containing up to $10^{-18}\ M_\odot$ per ejection. Even more to the point, CMEs are associated with flares and prominences (seen, of course, in Hα), often preceding major X-ray flares by tens of minutes (see review by Haisch, Strong, & Rodono 1991).

Can we scale up such events to an extremely active system such as Algol? Given that the same underlying physical process which produce solar flares, i.e., reconnection or relaxation of magnetic field geometry, are undoubtedly the cause of Algol's flares, there is every reason to expect CMEs on an enormous scale in the Algol system. First of all, the estimates of total mass in the two Algol X-ray flares seen so far can be easily estimated from the derived densities and emission measures as $\sim 10^{18-19}$ g. This is compared to the mass involved in the largest solar flares of about 10^{15-16} g, approximately the same as in the solar CME, or 3–4 orders of magnitude smaller than for Algol. If we assume a linear scaling for the CME mass, we obtain $\sim 5 \times 10^{-15}$ to $5 \times 10^{-14}\ M_\odot$ for an Algol CME. Given that two $\sim$several day monitoring observations of Algol with *EXOSAT* and *Ginga* both detected large flares, a flare rate of ~ 100 yr^{-1} is not out of the question, or a yearly CME mass ejection rate of $\sim 5 \times 10^{-13}$ to $5 \times 10^{-12}\ M_\odot$ yr^{-1}.

The largest uncertainty is in the amount of material that is actually captured by the primary. To get some estimate of this, we note that the velocities of CMEs reach up to 400–700 km s^{-1}, compared to 618 km s^{-1} for the escape velocity of the Sun. The comparison for the Algol K2 secondary is more favorable for mass loss, since its escape velocity is about 300 km s^{-1} (compared to 700 km s^{-1} for the Algol primary). Thus, if the MHD processes which produce the CME are similar to that on the Sun, it would not be surprising if much of the Algol CMEs matter escaped the secondary with some significant fraction ending up gravitationally bound to the primary star. Given that the rate of mass transfer required to produce the H II regions surrounding the primary is estimated by Richards (1992) to be $\gtrsim 10^{-11}\ M_\odot$ yr^{-1}, Algol CMEs may well be providing a significant fraction of the mass in the transient "disks" seen in the Algol system. In addition, the large velocities of the CME material compared to the stellar orbital velocities of 44 and 200 km s^{-1} could well be confusing the apparent "location" of some of the material as seen in radial velocity measurements.

7. CONCLUSIONS

Our *Ginga* X-ray monitoring of Algol has shown:

1. There are no dramatic changes in X-ray flux during *either* primary or secondary optical eclipse, with conservative upper limits of $\sim$20% and 10%, respectively, to any flux decrease in the 1.2–18 keV band.

2. From the *Ginga* observation and the previous *EXOSAT* observation of Algol, large ($\sim 10^{31}$ ergs s^{-1}) X-ray flares are not uncommon, possibly occurring as often as once per binary orbit.

3. The large flare observed with *Ginga*, although with similar peak temperature (≈ 65 MK) and emission measure ($\approx 10^{54}$ cm^{-3}) as the large *EXOSAT* flare, was of considerably longer duration, with a $1/e$ effective decay time of over 6 hr, roughly 4 times that of the earlier *EXOSAT* flare. This implies a nearly proportional increase in flare length scale, with a loop length of $\approx 6 \times 10^{11}$ cm, or a height of $2.9\ R_\odot = 0.8\ R_*$.

4. The strong and variable high-temperature Fe-line emission at 6.7 keV, also seen in other *Ginga* observations of large flares on UX Ari and II Peg, is not consistent with straightforward thin plasma thermal emission models. Line opacity or possibly temporal abundance variations in the flare plasma may be responsible for this phenomenon.

5. Mass ejections similar to solar coronal mass ejections, but on a much grander scale, are likely to be associated with large Algol flares. If such mass ejections occur once every few days, as suspected, they may contribute significant amounts of material to the transient H II or higher temperature plasma regions observed in the Algol system.

We wish to thank all the members of the *Ginga* LAC team at ISAS, elsewhere in Japan, and in the UK, without whose dedication this opportunity would not have been possible. We especially wish to thank F. Makino, K. Mitsuda, and K. Hayashida for their hospitality, understanding, and help with the *Ginga* data analysis software. We also acknowledge helpful discussions with T. Watanabe, K. Koyama, K. Makishima, T. Ohashi, T. Tsuru, M. Arnaud, J. Hughes, R. Corbet, C. Day, B. Haisch, K. Strong, and J. Lemen. R. A. S. was supported by NASA contract NAS8-37655 under the *Ginga* Visiting Investigator Program and by the Lockheed Independent Research Program.

REFERENCES

Acton, L. W. 1978, ApJ, 225, 1069
Allen, S. W., Fabian, A. C., Johnstone, R. M., Nulsen, P. E. J., & Edge, A. C. 1992, MNRAS, 254, 51
Batten, A. H., ed. 1989, Space Sci. Rev., 50, Nos. 1/2
Brandi, E., Garcia, L. G., Kondo, Y., & Sahade, J. 1989, A&A, 215, 331
Craig, I. J. D., McClymont, A. N., & Underwood, J. H. 1978, A&A, 70, 1
Cugier, H., & Molaro, P. 1984, A&A, 140, 105
Doyle, J. G., van den Oord, G. H. J., & Kellett, B. J. 1992, A&A, submitted
Doyle, J. G., et al. 1991, MNRAS, 248, 503
Eaton, J. A., & Hall, D. S. 1979, ApJ, 227, 907
Fisher, G. H., & Hawley, S. L. 1990, ApJ, 357, 243
Gibson, D. M. 1976, Ph.D. thesis, Univ. Virginia
Haisch, B. M. 1983, in Activity in Red Dwarf Stars, ed. P. B. Byrne & M. Rodono (Dordrecht: Reidel), 255
Haisch, B. M., Strong, K. T., & Rodono, M. 1991, ARA&A, 29, 275
Hall, D. S. 1989, Space Sci. Rev., 50, 219
Harnden, F. R., Fabricant, D., Topka, K., Flannery, B. P., Tucker, W. H., & Gorenstein, P. 1977, ApJ, 214, 418
Hayashida, K., et al. 1989, PASJ, 41, 273
Hjellming, R., & Gibson, D. M. 1980, in IAU Symp. 86, Radio Physics of the Sun, ed. M. R. Kundu & T. E. Gergeley (Dordrecht: Reidel), 209
Kopp, R. A., & Poletto, G. 1990, in Proc. Sixth Cambridge Workshop on Cool Stars, Stellar Systems, and the Sun, ed. G. Wallerstein (ASP Conf. Ser., 9), 119
Landini, M., & Monsignori-Fossi, B. C. 1975, A&A, 42, 213
Lestrade, J.-F., Mutel, R. L., Preston, R. A., & Phillips, R. B. 1988, ApJ, 328, 232
Makino, F., & ASTRO-C Team. 1987, Astrophys. Lett., 25, 223
Moore, R. L., et al. 1980, in Solar Flares, ed. P. Sturrock (Boulder: Colorado Associated Univ. Press), 341
Murakami, T., et al. 1989, PASJ, 41, 405
Pallavicini, R., et al. 1983, ApJ, 270, 270
Pasquini, L., Schmitt, J. H. H. M., & Pallavicini, R. 1989, A&A, 226, 225
Peres, G., Reale, F., Serio, S., & Pallavicini, R. 1987, ApJ, 312, 895
Peters, G. J., & Polidan, R. S. 1984, ApJ, 283, 745
Reale, F., Peres, G., Serio, S., Rosner, R., & Schmitt, J. H. H. M. 1988, ApJ, 328, 256
Richards, M. T. 1990, ApJ, 350, 372
———. 1992, ApJ, 387, 329
Richards, M. T., Mochnacki, S. W., & Bolton, C. J. 1988, AJ, 96, 326
Rosner, R., Tucker, W. H., & Vaiana, G. S. 1978, ApJ, 220, 643
Rothenflug, R., & Arnaud, M. 1985, A&A, 144, 431
Schnopper, H. W., et al. 1976, ApJ, 222, L119
Stern, R. A., Uchida, Y., Walter, F., Vilhu, O., Veale, A., Hannikainen, D., Brown, A., & Haisch, B. M. 1992, ApJ, 391, 760
Stern, R. A., Underwood, J. H., & Antiochos, S. K. 1983, ApJ, 264, L55
Strassmeier, K. G., Hall, D. S., Zeilik, M., Nelson, E., Eker, Z., & Fekel, F. C. 1988, A&AS, 72, 291
Swank, J. H., White, N. E., Holt, S. S., & Becker, R. H. 1981, ApJ, 246, 208
Sylwester, J., Lemen, J. R., & Mewe, R. 1984, Nature, 310, 665
Tsuru, T., et al. 1989, PASJ, 41, 679
Turner, M. J. L., et al. 1989, PASJ, 41, 345
van den Oord, G. H. J., & Mewe, R. 1989, A&A, 213, 245
van den Oord, G. H. J., Mewe, R., & Brinkman, A. C. 1988, A&A, 205, 181
Vesecky, J. F., Antiochos, S. K., & Underwood, J. H. 1979, ApJ, 233, 987
Walter, F. M., & Bowyer, S. 1981, ApJ, 245, 671
White, N. E., Culhane, J. L., Parmar, A. N., Kellett, B. J., Kahn, S., van den Oord, G. H. J., & Kuijpers, J. 1986, ApJ, 301, 262
White, N. E., Holt, S. S., Boldt, E. A., & Serlimitsos, P. J. 1980, ApJ, 239, L69